Small-Angle X-ray Scattering Studies of Peptide–Lipid Interactions Using the Mouse Paneth Cell α-Defensin Cryptdin-4

Abhijit Mishra,[*] Kenneth P. Tai,[†] Nathan W. Schmidt,[*,‡,§]
André J. Ouellette,[†] *and* Gerard C. L. Wong[*,‡,§]

Contents

[*] Department of Bioengineering, University of California, Los Angeles, California, USA
[†] Department of Pathology and Laboratory Medicine, USC Norris Cancer Center, Keck School of Medicine of the University of Southern California, Los Angeles, California, USA
[‡] Department of Physics, University of Illinois, Urbana-Champaign, Illinois, USA
[§] Department of Materials Science, University of Illinois, Urbana-Champaign, Illinois, USA

Abstract

In the presence of specialized proteins or peptides, a biological membrane can spontaneously restructure itself to allow communication between the intracellular and the extracellular sides. Examples of these proteins include cell-penetrating peptides and antimicrobial peptides (AMPs), which interact with cell membranes in complex ways. We briefly review cell-penetrating peptides and AMPs, and describe in detail how recombinant AMPs are made and their activity evaluated, using α-defensins as a specific example. We also review X-ray scattering methods used in studying peptide–membrane interactions, focusing on the procedures for small-angle X-ray scattering experiments on peptide–membrane interactions at realistic solution conditions, using both laboratory and synchrotron sources.

1. INTRODUCTION

With the exception of solute uptake by selective transmembrane pumps and transporters or endocytosis of receptor-bound ligands, biological membranes remain impervious to protein molecules. However, certain cell-penetrating peptides (CPPs), including the HIV TAT protein transduction domain (Frankel and Pabo, 1988; Green and Loewenstein, 1988), a short domain in the Drosophila *antennapaedia* homeotic transcription factor (Antp) (Joliot *et al.*, 1991), and the Herpes-Simplex-Virus-1 DNA binding protein VP22 (Elliott and O'Hare, 1997), enable spontaneous membrane restructuring, to allow molecules to traverse the boundary between the intracellular and extracellular sides. Antimicrobial peptides (AMPs) comprise a different set of host defense molecules with membrane disruptive activities, highly diverse primary and secondary structures. Most CPPs and AMPs are cationic and associate with electronegative microbial cell membranes via electrostatic interactions. They also have varying degrees of hydrophobicity and are therefore amphiphilic. The hydrophobic side chains perturb membrane self-assembly and stability, although the detailed molecular mechanisms of action have not been fully understood. Here, we describe X-ray scattering methods and illustrate their application in characterizing membrane interactions with the bactericidal α-defensin, cryptdin-4 (Crp4), in small-angle X-ray scattering (SAXS) experiments performed in solution using both laboratory and synchrotron sources.

1.1. Cell-penetrating peptides

CPPs are short (<20 amino acid) cationic peptides that can traverse cell membranes of various mammalian cells. A wide variety of macromolecules can be internalized while retaining their biological activity when attached to

these peptides. This ability of CPPs to transport biologically active molecules across cell membranes makes them promising candidates for a broad range of drug–delivery applications. The CPPs can be classified into arginine–rich peptides and amphipathic peptides. The arginine–rich CPPs have been the most widely studied (El-Sayed *et al.*, 2009; Wender *et al.*, 2008). The exact molecular mechanism of cellular entry of arginine–rich CPPs is currently an active area of research. The cationic nature of the peptides is a necessary but not sufficient condition for translocation activity. It has been observed that arginine–rich oligomers can enter cells, but similar length polymers composed of other basic amino acids such as lysine, ornithine, or histidine cannot (Mitchell *et al.*, 2000). The guanidinium headgroup of arginine with its ability to form bidentate hydrogen bonds is the central structural feature required for peptide uptake (Rothbard *et al.*, 2005), and recent work suggests that such hydrogen bond patterns is related to the generation of specific types of membrane curvature topologically required for pore formation (Mishra *et al.*, 2008; Schmidt *et al.*, 2010b).

Experimental studies have shown evidence for many different entry mechanisms, including direct translocation and various endocytotic mechanisms. It is believed that more than one mechanism may be involved in translocation activity, with the dominant mechanism influenced by a variety of factors, including temperature, incubation time, cell type, cargo type and size, and linkage type and size (Wender *et al.*, 2008).

1.2. Antimicrobial peptides

AMPs are important mediators of an innate host defense system, with antimicrobial activities against a broad spectrum of microorganisms (Brogden, 2005; Hancock and Sahl, 2006; Shai, 1999; Zasloff, 2002). Most AMPs share two general structural features; they are amphipathic and cationic (Brogden, 2005; Zasloff, 2002). It is believed that AMPs disrupt membranes through a combination of electrostatic interactions between cationic amino acid side chains and electronegative components of the microbial cell envelope, followed by the insertion of hydrophobic patches into the nonpolar interior of the membrane bilayer (Brogden, 2005; Huang, 2000; Matsuzaki, 1999; Matsuzaki *et al.*, 1998; Shai, 1999; Zasloff, 2002).

Defensins constitute one of two major AMP families in mammals (Ganz, 2003; Lehrer, 2004; Selsted and Ouellette, 2005), the other being the cathelicidins (Zanetti, 2004). Defensins were among the first AMPs to be described (Lehrer *et al.*, 1983; Selsted *et al.*, 1983), consisting of three subfamilies of cationic, Cys-rich AMPs, the α–, β–, and θ–defensins, all of which have broad-spectrum antimicrobial activities and are defined by the disulfide connectivities (Selsted and Ouellette, 2005). The α–defensins are major granule constituents of mammalian phagocytic leukocytes and of

small intestinal Paneth cells (Ganz, 2003). The β-defensins, discovered in cattle as AMPs of airway and lingual epithelial cells, and in bovine neutrophil granules (Diamond *et al.*, 1991; Schonwetter *et al.*, 1995; Selsted *et al.*, 1993), exist in diverse species and are expressed by many epithelial cell types and more widely than the α-defensins (Schutte *et al.*, 2002). The θ-defensins are unusual ∼2 kDa peptides from rhesus macaque neutrophils and monocytes and are found only in Old World monkeys. θ-Defensins are the only macrocyclic peptides known in animals, and like all defensins, they are stabilized by three disulfide bonds. θ-Defensins assemble from two hemiprecursors that derive from α-defensin genes that have stop codons that terminate the peptide at residue position 12. The ligation mechanisms that circularize the closed θ-defensin polypeptide chain remain unknown.

1.3. α-Defensins

α-Defensins are ∼4 kDa, cationic, and amphipathic peptides with broad-spectrum bactericidal activities. Structurally, they consist of a triple-stranded β-sheet structure that is established by three invariantly paired disulfide bonds (Fig. 4.1) (Lehrer, 2007). Despite having highly diverse primary structures (Ouellette, 2006; Ouellette and Bevins, 2001), α-defensins retain conserved biochemical features that include an invariant disulfide array (Selsted and Harwig, 1989), a canonical Arg–Glu salt bridge, a conserved
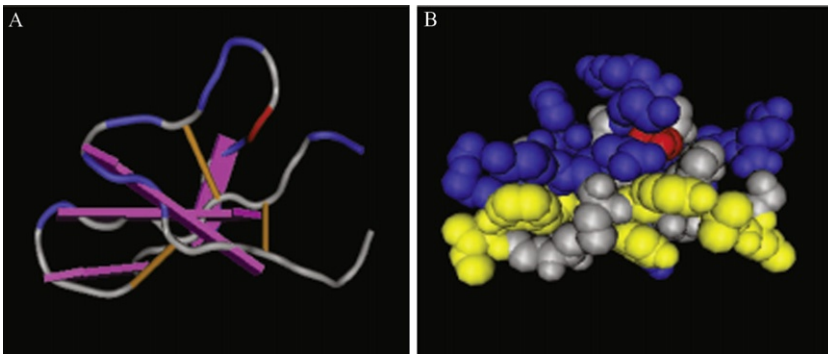
Figure 4.1 Solution structure of mouse Paneth cell alpha–defensin Crp-4 (protein data bank ID 2GW9) obtained by NMR. (A) Structure shown in worm rendering. The three disulfide bonds from six cysteines are displayed in orange and Beta-sheets are represented by purple arrows. Blue regions denote cationic amino acids (arginine, lysine, and histidine), while the anionic glutamic acid is red. (B) Space-filled structure illustrates the cationic (blue) and hydrophobic (yellow) patches of amphipathic Crp-4. Here, hydrophobic amino acids include leucine, isoleucine, valine, phenylalanine, and tyrosine. Neutral residues are colored gray.

Gly residue at CysIII+8, and high Arg content relative to Lys (Lehrer, 2007). Studies have shown consistently that bactericidal activity is independent of these highly conserved features of the peptide family, with exception to the relatively high Arg content (Lehrer *et al.*, 1988; Maemoto *et al.*, 2004; Rajabi *et al.*, 2008; Rosengren *et al.*, 2006; Wu *et al.*, 2005).

In vitro, α–defensins are microbicidal against gram–positive and gram–negative bacteria, fungi, spirochetes, protozoa, and enveloped viruses (Aley *et al.*, 1994; Borenstein *et al.*, 1991; Ganz *et al.*, 1985; Lehrer, 2007; Zhu, 2008). Most α–defensins exert antibacterial effects by membrane disruption, inducing permeabilization of target cell membranes as inferred from the formation of transient defects or stable pores in model phospholipid bilayers (Hristova *et al.*, 1996; White *et al.*, 1995). For example, the bactericidal activity of the mouse α–defensin cryptdin–4 (Crp4) is directly related to peptide binding and disruption of phospholipid bilayers (Satchell *et al.*, 2003a). Crp4 exhibits strong interfacial binding to model membranes, inducing "graded" fluorophore leakage from model membrane vesicles (Cummings and Vanderlick, 2007; Cummings *et al.*, 2003; Satchell *et al.*, 2003b). Mammalian α–defensins secreted by Paneth cells determine the composition of the mouse small intestinal microbiome, apparently by selecting for peptide-tolerant microbial species as residents in that microbial ecosystem.

1.4. Peptide-induced membrane restructuring

The HIV TAT cell-penetrating peptide generates negative Gaussian membrane curvature in model membrane systems manifested in the generation of a Pn3m cubic phase. This type of curvature, also known as "saddle-splay" curvature, is characterized by saddle-shaped deformations. The ability of the guanidinium group of arginine to crosslink multiple lipid headgroups through bidentate hydrogen bonding facilitates the generation of negative Gaussian curvature (Mishra *et al.*, 2008). The negative Gaussian curvature, necessary to form the observed cubic phases, is topologically required for pore formation, and induction of that curvature can lower the free energy barriers, providing a range of entry mechanisms, including direct translocation as well as endocytotic pathways (Schmidt *et al.*, 2010b).

The generation of negative Gaussian curvature correlates with the permeation capability of a peptide. The arginine-rich cell–penetrating peptides, Antp and polyarginine, also induce negative Gaussian curvature, but polylysine (K_8), which has the same charge as TAT but cannot form bidentate hydrogen bonds, generates negative mean curvature but zero Gaussian curvature, resulting in inverted hexagonal H_{II} phases. In general, the interaction between charged polymers and charged membranes yields a rich polymorphism of phases with a broad range of applications (Liang *et al.*, 2005; Purdy Drew *et al.*, 2008; Rädler *et al.*, 1997; Wong *et al.*, 2000; Yang *et al.*, 2004).

The structural tendency to form negative Gaussian membrane curvature has also been observed in pore-forming AMPs and synthetic peptide mimics. Under specific lipid compositions and solution conditions, alamethicin (Keller *et al.*, 1996), gramicidin S (Prenner *et al.*, 1997; Staudegger *et al.*, 2000), lactoferricin (LF11)-derived peptides, VS1–13 and VS1–24 (Zweytick *et al.*, 2008), as well as protegrin-1 and peptidyl-glycylleucine-carboxyamide (Hickel *et al.*, 2008), also induce cubic phases. Defensins also restructure vesicles by inducing negative Gaussian curvature when the lipid composition of model membranes mimics that of bacterial membranes but not the composition of mammalian membrane bilayers (Schmidt *et al.*, 2010a). Likewise, curvature generation drives the formation of a sequence of phases, including cubic and hexagonal phases for synthetic molecules that mimic AMP action (Yang *et al.*, 2007, 2008). The preferential formation of high curvatures necessary for pore formation is favored in membranes rich in negative curvature lipids, such as those found in high concentrations in bacterial membranes (Som *et al.*, 2009; Yang *et al.*, 2008). The generation of negative Gaussian curvature requires both anionic and negative curvature lipids. Model membranes in water form bilayers in the absence of AMPs. The peptides interact differently with membranes of pure lipid species. For example, membranes composed of pure anionic lipids are "glued" together into a lamellar phase; membranes of pure negative curvature lipids interact weakly with peptides with no major reorganization of lipids. The induced phases have zero Gaussian curvature, in contrast to the behavior of composite membranes.

The methods outlined in this chapter are general, applicable to a broad range of AMPs and CPPs. Here, we focus on Crp4 as a model of peptide–membrane interactions. In order to elucidate the molecular mechanisms responsible for the bacterial killing activity, we investigate peptide–membrane interactions using SAXS. Below, we examine why and how X-rays are used for this purpose.

2. X-Rays as Structural Probes of Biological Systems Under Biomimetic Conditions

Historically, diffraction (or equivalently, "scattering")-based methods have contributed immensely to our understanding of structures at the nanoscale. Ideally, the scattering particle should interact only weakly with the system under study and its wavelength must be comparable to the length scale of the system (Chaikin and Lubensky, 1995). Electrons are scattered by the electrostatic forces between the electrons and the atoms within the system and require energies of $\sim$100 eV to probe nanoscale structures. However, typically, thin ($\sim$1 µm thick) samples are needed to prevent

problems with multiple scattering. Moreover, electron-based probes typically require a vacuum, which is quite different from physiological conditions. However, this problem is sometimes partially circumvented through differential pumping. Neutrons have a much higher mass than electrons and hence require much lower energies (~ 0.1 eV) to probe nanostructures. Neutrons are scattered by nuclear forces or by the electron spins. They interact weakly with matter and have low absorption. Therefore, neutrons can penetrate samples several millimeters thick. However, because of this, large amounts of samples are needed for neutron scattering which is not always feasible for biological samples, such as the samples considered here. Also, neutron sources are relatively weak, with the flux of neutrons much lower than X-rays. X-ray photons with energy $\sim 10^4$ eV have wavelengths in the angstrom range; suitable for studying nanostructures. These X-rays can penetrate matter up to a millimeter and therefore provide "bulk" information. X-ray scattering also requires much lower sample amounts compared to neutron scattering. In addition, X-ray scattering experiments on biological macromolecules can be performed under near-physiological conditions, enabling us to examine their structural response to changes in a variety of parameters (e.g., pH, ionic strength, concentrations, temperature, etc.) Aside from studies of biomembrane-based systems, X-ray diffraction techniques can also be used to study other weakly scattering systems such as biopolymer-based systems under physiologically relevant conditions (Purdy et al., 2007; Sanders et al., 2005, 2007; Wong, 2006).

2.1. X-ray diffraction of weakly ordered systems

Most biological systems are not ordered into crystals. For example, membrane-based systems differ from conventional solid-state crystalline materials in that they are often weakly ordered, exhibiting only one-dimensional or two-dimensional periodicity rather than the three-dimensional periodicity of crystals. In this sense, they are analogous to liquid crystals. These systems are fluid and their periodic density distributions have much greater contributions from thermal fluctuation compared to crystalline samples. In the characterization of lipid-based systems by diffraction, two regions of the diffraction pattern are used to identify the structure. The small-angle region identifies the symmetry and long-range organization of the phase, while the wide-angle region gives information on the molecular packing or short-range organization of the phase (Seddon and Templer, 1995). The diffraction signals from these systems are in general weaker than those from crystals. Moreover, the molecular constituents of biological molecules are generally composed of combinations of mostly low Z elements, such as carbon, hydrogen, and oxygen, which make the electron density contrast between the constituent components low and thus lead to weak diffraction

intensities. The collection of interpretable data from such systems, there-
fore, is facilitated by X-ray sources with high intensity and high resolution.

2.2. Synchrotron X-ray sources

Synchrotron radiation is produced by charged particles traveling at relativistic
speeds forced to travel along curved paths by applied magnetic fields. High-
speed electrons circulating at constant energy in synchrotron storage rings
produce X-rays. X-rays can also be produced in insertion devices, like
wigglers or undulators, situated in the straight sections of storage rings.
Alternating magnetic fields in these devices force the electrons along oscillat-
ing paths in the horizontal plane instead of straight lines, greatly enhancing the
intensity of radiation. A wiggler consists of a series of magnets that force the
electrons to turn in alternating in-plane directions for a fixed number of
spatial periods. The intensity of the radiation from each wiggle is added up
and the resultant intensity is proportional to the number of wiggles. Undu-
lators also have a series of magnets; however, the radiation emitted from one
undulation is in phase with the radiation from subsequent undulations. The
resultant intensity is therefore proportional to the square of the number of
undulations. The coherent addition of amplitudes is only valid at one partic-
ular wavelength; hence, radiation from undulators is quasi-monochromatic.

2.3. Theory of X-ray diffraction

In the classical description, X-rays are transverse electromagnetic waves,
where the electric and magnetic fields are perpendicular to each other and
to the direction of propagation. It is characterized by its wavelength λ, or its
wavenumber $k = 2\pi/\lambda$. From a quantum mechanical perspective, the
X-rays can be viewed as a beam of photons, with each photon having an
energy $\hbar\omega$ and momentum $\hbar\mathbf{k}$. The intensity of the beam is given by the
number of photons passing through a given area per unit time. When
X-rays interact with a free scatterer with charge q and mass m, the scattered
intensity I_{sc} at distance R from the scatterer is

$$I_{sc} = I_0 \frac{q^4}{m^2 c^4 R^2} \left(\frac{1 + \cos^2 2\theta}{2} \right) \tag{4.1}$$

where I_0 is the incident beam intensity, c is the velocity of light, and 2θ is the
scattering angle. Protons and electrons have the same charge, but the mass of
a proton is 1836 times larger than that of an electron. The scattered intensity
by a proton is, therefore, $(1836)^2$ times smaller than that by an electron.
Hence, the X-ray scattering pattern is predominantly contributed by the
interactions between X-rays and electrons, and the scattering contrast is due

to the electron density difference within the system. When electrons scatter X-rays, if the wavelength of the scattered wave is the same as that of the incident one, the scattering process is called *elastic*. However, if energy is transferred to the electron, the scattered photon has a longer wavelength relative to that of the incident photon, and the scattering process is *inelastic*. In this chapter, we are primarily concerned with elastic scattering.

In an X-ray diffraction experiment, the detectors usually count the number of scattered photons. The measured intensity, I_{sc}, is the number of photons per second recorded by the detector. The differential cross-section ($d\sigma / d\Omega$) can be defined as

$$\frac{d\sigma}{d\Omega} = \frac{\text{(number of X-ray photons scattered per second in } d\Omega)}{\text{(incident flux)} d\Omega} \quad (4.2)$$

where σ is the scattering cross-section, $d\Omega$ is the solid angle subtend by the detector, and incident flux is the incident beam intensity (I_0) divided by its cross-section area (A_0). The measured intensity, I_{sc}, is related to the differential cross-section $d\sigma / d\Omega$ by

$$\left(\frac{d\sigma}{d\Omega}\right) = \frac{I_{SC}}{(I_0/A_0) d\Omega} \quad (4.3)$$

or

$$I_{sc} = \frac{I_0}{A_0}\left(\frac{d\sigma}{d\Omega}\right)(d\Omega) \quad (4.4)$$

From the theory of X-ray scattering (Als-Nielsen and McMorrow, 2001; Guinier, 1994; Warren, 1990), the differential cross-section for a system at thermal equilibrium:

$$\frac{d\sigma}{d\Omega} \propto P(q)|f(q)|^2 S(q) \quad (4.5)$$

where $P(q)$ is the polarization factor, $f(q)$ is the form factor of the scatterer, and $S(q)$ is the structure factor for the scatterer lattice. $q = \mathbf{k}_s - \mathbf{k}_i$, is the scattering vector which measures the photon momentum transfer ($\mathbf{k}_i$ and $\mathbf{k}_s$ are the wavevectors of the incident and scattered waves, respectively). For elastic X-ray scattering, the scattering vector q is given by

$$|q| = \frac{4\pi \sin\theta}{\lambda} = \frac{2\pi}{d} \quad (4.6)$$

where λ is the wavelength of the incident X-ray, θ is the half of the scattering angle, and d is the periodicity of the electron density fluctuation.

The polarization factor $P(q)$ depends on the X-ray source. In a synchrotron source, the electrons orbit in the horizontal plane and hence, the emitted X-rays are linearly polarized in the orbit plane but elliptically polarized when viewed out of that plane. So, for synchrotron source, polarization factor $P(q) = 1$ in the vertical scattering plane, while $P(q) = \cos^2 2\theta$ in the horizontal scattering plane where 2θ is the scattering angle. For an unpolarized X-ray source, the polarization factor $P(q) = (1 + \cos^2 2\theta)/2$. For the SAXS ($2\theta < 10°$), the polarization factor is not significantly different from $P(q) \sim 1$.

The static structural factor $S(q)$ accounts for the geometry of scatterer and contains the structural information of the biomolecular system.

$$S(q) = \frac{1}{N} \sum_{i,j}^{N} \left\langle e^{iq[ri(0) - rj(0)]} \right\rangle = \frac{V}{N} \int dr G(r) e^{-iqr} \qquad (4.7)$$

and,

$$G(r) = \frac{1}{V} \int dr' \langle \rho(r).\rho(r + r') \rangle \qquad (4.8)$$

$G(r)$ is the density–density correlation function, with $\rho(r)$ being the electron density distribution of the system.

The form factor $f(q)$ of the scatterer is the Fourier transform of its electron density. For an atom, $f(q) = -r_0 f^0(q)$, where r_0 is the Thomson scattering length ($r_0 = 2.82 \times 10^{-5}$Å) and $f^0(q)$ is the atomic form factor given by

$$f^0(q) = \int \rho(r) e^{iq \cdot r} dr = \begin{cases} z, & \text{for } q \to 0 \\ 0, & \text{for } q \to \infty \end{cases} \qquad (4.9)$$

where $\rho(r)$ is the number density of electron at position r around the nucleus in the atom and z is the total number of electrons in the atom.

For a molecule, the form factor $f^{\text{mol}}(q)$ is

$$f^{\text{mol}}(q) = -r_0 \sum_{r_j} f_j(q) e^{iq \cdot r_j} \qquad (4.10)$$

where $f_j(q)$ is the atomic form factor of the jth atom in the molecule. If $|f^{\text{mol}}(q)|^2$ can be determined experimentally with sufficient values of scattering vectors q, the position r_j of the jth atom in the molecule can be known.

For an ordered arrangement of atoms or molecules (e.g., a crystal), the form factor $f^{\text{crystal}}(q)$ is

$$f^{\text{crystal}}(q) = -r_0 \left(\sum_{r_j} f_j^{\text{mol}}(q) e^{iq \cdot r_j} \right) \left(\sum_{R_n} e^{iq \cdot R_n} \right) \qquad (4.11)$$

where the first term is the scattering amplitude from the basis of the molecules or atoms contained in the unit cell and is known as the "unit cell structure factor", in which r_j is the position of jth molecule or atom in the unit cell, and the second term is a sum over lattice sites and is known as the "lattice sum." All the terms in the lattice sum are phase factors located on the unit circle in a complex plane. This lattice sum and as a result, the crystal's form factor f^{crystal} is nonvanishing if and only if the scattering vector q coincides with a reciprocal lattice vector G which satisfies $G \cdot R_n = 2\pi \times m$, where m is an integer. This is the Laue condition for the observation of X-ray diffraction. Scattering from a crystal is confined to distinct points in the reciprocal space. The scattering signature can therefore be used to deduce structural information.

3. PREPARATION OF PEPTIDE–LIPID COMPLEXES FOR X-RAY MEASUREMENTS

3.1. Preparation of recombinant α-defensins

Recombinant α-defensins are expressed in *Escherichia coli* as N-terminally linked, 6×-histidine-tagged fusion peptides as described (Figueredo *et al.*, 2010; Satchell *et al.*, 2003b; Shirafuji *et al.*, 2003). α-Defensin cDNA coding sequences are amplified and directionally subcloned from cDNAs into a pET28a protein expression vector (Novagen, Inc., Madison, WI, USA). For example, Crp4 was amplified from mouse cDNA corresponding to nucleotides 182–274, and directionally subcloned into the *Eco*RI and *Sal*I restriction sites of pET28a. The Crp4 cDNA sequence was amplified using the forward primer, 5′-GCG CGA ATT CCA TCG AGG GAA GGA TGG GTT TGT TAG CTA TTG T, and paired with the reverse primer, 5′-ATA TAT GTC GAC TCA GCG ACA GCA GAG CGT GTA CAA TAA ATG. For expression of peptides that lack Met, forward primers incorporate a Met codon immediately 5′- of the peptide coding sequence, providing a unique cyanogen bromide (CNBr) cleavage site for subsequent separation of the defensin molecule from the pET-28-encoded, His-tag fusion partner. For example, Crp4 is Met-free, so the CNBr reaction does not cleave within the polypeptide chain. However, for Met-containing

α-defensins, the CNBr cleavage site is replaced with enzymatic cleavage sites for enterokinase or thrombin.

α-Defensin constructs are transformed into *E. coli* BL21(DE3)–Codon–Plus–RIL cells (Stratagene, La Jolla, CA, USA), whose additional Arg codons help to minimize *E. coli* codon bias for Arg-rich defensins. For induction purposes, 6 L Terrific Broth (TB) culture medium is prepared as follows: 12 g of BactoTryptone (BD biosciences, San Jose, CA, USA), 24 g of BactoYeast Extract (BD), and 4 mL of glycerol are combined with 900 mL of deionized water, and all solids are dissolved before autoclaving. The following sterile solution components are added to the medium: 100-mL phosphate buffer (0.17 M KH_2PO_4 and 0.72 M K_2HPO_4), 5-mL 30% dextrose, and kanamycin to a final concentration of 70 μg/mL. *E. coli* are grown to mid–log phase (OD_{600} nm = 0.6–0.9) at 37 °C TB and induced by addition of isopropyl-β-D-1-thiogalactopyranoside to 0.1 m*M*. The bacterial cells are harvested after 4–6 h or after growth, transferred to 1–L wide–mouth polycarbonate centrifuge bottles, and deposited by centrifugation at 5500×g for 10 min at 4 °C in a FIBERLite F8-4X1000Y rotor (FIBERLite Centrifuge, Santa Clara, CA, USA) in a Sorvall RC–26 Plus Superspeed centrifuge. Deposited cells are stored at −20 °C. Bacterial cell pellets resuspended in 6–*M* guanidine–HCl and 100–m*M* Tris–HCl (pH 8.1) are sonicated (70% power, 50% duty cycle for 2 min using a Branson Sonifier 450). Lyzates are clarified by centrifugation at 25,000×g for 30 min at 4 °C in a FIBERLite F21-8X50 rotor using rotor code SA-600 in a Sorvall RC–26 Plus superspeed centrifuge.

3.2. Purification of recombinant α-defensins

His-tagged fusion peptides are purified using nickel–nitrolotriacetic acid (Ni–NTA, Qiagen) resin affinity chromatography. Cell lyzates are incubated with resin at 4 °C overnight at a ratio of 25:1 (v/v) in 6–*M* guanidine–HCl in 100–m*M* Tris–HCl (pH 8.1). The His-tagged fusion peptides are eluted with approximately 10 bed vol of 1–*M* imidazole, 6–*M* guanidine–HCl, and 20–m*M* Tris–HCl (pH 6.5), dialyzed in SpectraPor 3 (Spectrum Laboratories, Inc., Rancho Dominquez, CA, USA) membranes, using three exchanges of 4 L of 5% acetic acid. The dialyzed peptides are lyophilized, dissolved in 80% formic acid, and solid CNBr is added to 10 mg/mL. The peptides are placed in polypropylene tubes, gently purged by a stream of N_2 gas, sealed, foil–wrapped, and incubated at ambient temperature overnight. The cleavage reaction is terminated by the addition of 10 vol of H_2O and lyophilized. Peptide lyophilate is dissolved in 5% acetic acid, centrifuged 15 min at 15,000×g in a microcentrifuge, and sterilized through a 0.22-μm filter.

Recombinant α-defensins are purified to homogeneity by reverse-phase high performance liquid chromatography (RP-HPLC). The peptide is

initially purified from the 36 amino acid 6×–histidine-tag fusion partner on a semipreparative C18 column (Vydac 218TP510) at a 15–45% linear gradient of acetonitrile (0.1% trifluoroacetic acid (TFA) is used as the ion-pairing agent in the mobile phase). The peptides are further purified through an analytical C18 column (Vydac 218TP54), and homogeneity is assessed by using acid–urea polyacrylamide gel electrophoresis (AU-PAGE). AU-PAGE is a superior method for determining defensin homogeneity, because small cationic peptides are resolved on the basis of their electropositive charge–to-size ratios. Misfolded peptide variants display reduced mobilities relative to native peptides, providing an index of peptide quality. Peptide masses are confirmed by MALDI-TOF mass spectrometry.

3.3. Refolding of recombinant and synthetic peptides

Certain recombinant α–defensins such as Crp4 are produced within *E. coli* as properly folded peptides with correct disulfide pairings. Occasionally, however, certain recombinant and synthetic α–defensin peptides require reduction and refolding procedures to eliminate disulfide mispairings and insure proper disulfide linkages (Cys$^{I–VI}$, Cys$^{II–IV}$, Cys$^{III–V}$). Assessing proteolytic sensitivity provides a rapid test of whether an expressed α–defensin is correctly folded or not. α–Defensins are inherently resistant to proteolysis by trypsin, and disulfide mispairings render the peptide sensitive to tryptic cleavage. Lyophilized peptides dissolved in 6-M guanidine HCl, 0.2-M Tris base, and 2-mM sodium EDTA (pH 8.2) at peptide concentrations ranging from 0.5 to 2 mg/mL are purged under N_2, sealed, and denatured at 50 °C for 30 min. Following denaturation, 5-mol dithiothreitol per mol polypeptide Cys is added to the peptide solution. The reduction reaction mixture is purged briefly with N_2, incubated at 50 °C for 4 h, and then purified through RP-HPLC on a semipreparative C18 column. The extent of peptide reduction is confirmed by MALDI-TOF MS as an increase in peptide mass of six atomic mass units (a.m.u.). Reduced peptides are concentrated to ∼1–6 mL by vacuum centrifugation in a SpeedVac® SC210A and diluted to concentrations of 0.1–0.3 mg/mL peptide with 0.1-M NH_4HCO_3, 2.0-mM EDTA, 0.1-mg/mL cysteine, 0.1-mg/mL cysteine (pH 7.8–8.0), and purged with N_2. The peptide refolding mixture is adjusted to pH 7.8–8.0 by dropwise addition of NH_4OH, purged again with N_2, sealed, and gently stirred at 4 °C. Samples (∼0.1%) of the refolding mixture are assessed for correct folding at intervals by analytical RP-HPLC. As α–defensins fold, exposure of hydrophobic residues is reduced and the retention time on analytical RP-HPLC decreases. When refolding peptide mixtures are separated on semipreparative C18 RP-HPLC, the first peptide peak to elute is the correctly folded peptide in our experience.

3.4. Microbicidal peptide assays

α-Defensins are tested for microbicidal peptide activity against a panel of microorganisms. Exponential-phase bacteria are grown in trypticase soy broth (TSB). Microbes are deposited by centrifugation at 10,000×g for 3 min and washed three times with 10-mM PIPES (pH 7.4), supplemented with 1% (v/v) of respective growth medium (10-mM PIPES-TSB) and resuspended in PIPES-TSB). Approximately 1–5 × 10^6 CFU/mL of bacteria or fungi are incubated with peptides at various concentrations in a total volume of 50 μL. For assays of peptides other than Crp4, the most bactericidal known mouse α-defensin, is used as a positive control peptide, and cells suspended in 10-mM PIPES-TSB without added peptide provide negative controls. The test samples are incubated at 37 °C with shaking for 1 h, and 20-μL samples of incubation mixtures are diluted 1:2000 in 10-mM PIPES (pH 7.4) and plated on TSB agar plates using an Autoplate 4000 (Spiral Biotech Inc., Bethesda, MD, USA). After incubation overnight at 37 °C, bacterial cell survival is determined by counting CFU.

Results from a typical bactericidal peptide assay are shown in Fig. 4.2. Here, the activity of mouse Crp4 against *E. coli* ML35 cells was compared with that of its inactive precursor, proCrp4. The data show that Crp4 exposure reduces *E. coli* cell survival by 99.9% at concentrations of 1.5 μM or less, and it shows
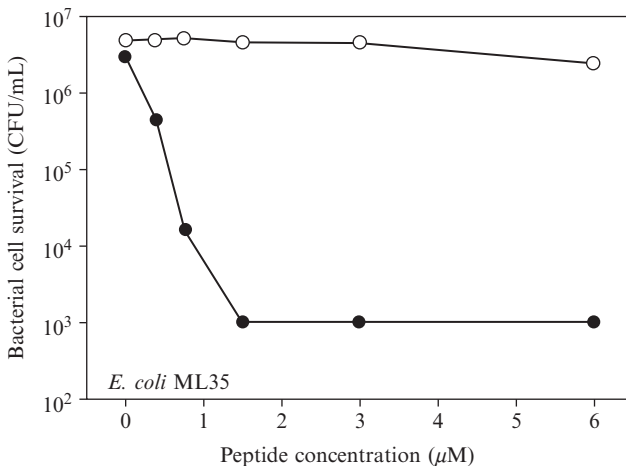
Figure 4.2   Bactericidal peptide activity of recombinant Crp4 (●) and the inactive pro-α-defensin, proCrp4 (○). *E. coli* ML35 cells were incubated with peptides in 50 μL of 10-mM PIPES, pH 7.4, 1% TSB (TSB, v/v) for 1 h at 37 °C at the concentrations shown. Following peptide exposure, incubation mixtures were plated on a semisolid medium and incubated for 16 h at 37 °C. Surviving bacterial cells were quantitated as colony-forming units (CFU)/mL. Cell survival values of 1 × 10^3 CFU/mL or less indicate that no colonies were detected after overnight growth.

minimal cytotoxic effects on mammalian cells in culture at levels of 100-μ g/mL peptide (data not shown). In contrast, the proCrp molecule lacks bactericidal peptide activity under these conditions due to the inhibitory effects of its anionic proregion. Previous studies have shown that Crp4 bactericidal effects occur by an undisclosed membrane disruptive mechanism, and consistent with its lack of activity, proCrp4 does not interact with or disrupt model membranes. Thus, the Crp4 molecule provides a useful peptide for studying peptide–lipid interactions using SAXS approaches.

3.5. Vesicle preparation

To investigate how AMPs interact with membranes, we examine the structure and interactions of corresponding peptide–lipid complexes. Small unilamellar vesicles (SUVs) of different compositions are used for X-ray diffraction experiments. The lipids 1,2-dioleoyl–sn–glycero-3-[phospho-L-serine] (sodium salt) (DOPS), 1,2-dioleoyl–sn–glycero-3-phosphocholine (DOPC), 1,2-dioleoyl–sn–glycero-3-phosphoethanolamine (DOPE), and 1,2-dioleoyl–sn–glycero-3-[phospho-rac-(1-glycerol)] (sodium salt) (DOPG) are purchased from Avanti Polar Lipids and used without further preparation. Mixtures of DOPG and DOPE can be used as an approximate model for bacterial membranes, and DOPS, DOPC, and DOPE mixtures can be used to model eukaryotic membranes. Stock solutions of lipids in chloroform are mixed at the desired ratios, dried under N_2, and desiccated under vacuum overnight. The dried lipids are rehydrated with Millipore H_2O (Tris/HEPES buffer may also be used) to a final concentration of 30 mg/mL and incubated at 37 °C overnight. This solution is sonicated to clarity and extruded through a 0.2-μm Nucleopore filter to make liposomes. Freshly prepared liposomes may be stored at 4 °C and should be used within a week.

The peptides are dissolved in Millipore H_2O at 5 mg/mL. The peptide solutions are mixed with liposomes at different peptide–lipid molar ratios and sealed in 1.5-mm quartz capillaries, which typically have 10-μm thick walls. These samples are typically incubated at least 24 h before data collection.

3.6. Data collection

The sample-containing X-ray capillaries are placed in the incident X-ray beam and the scattered X-rays are collected using a two-dimensional detector. Figure 4.3 shows a typical layout of a SAXS system. X-rays generated at the source are focused and collimated, passing through the presample flightpath. The length of the postsample flightpath depends on the q range of interest in the experiment. SAXS data at Stanford Synchrotron Radiation Laboratory (Palo Alto, CA) (BL4-2) Advanced Light Source (Berkeley, CA BL-7.3.3) and Advanced Photon Source (Argonne, IL, BESSRCAT BL-12ID) are collected using 9-, 10- and 12-keV X-rays,
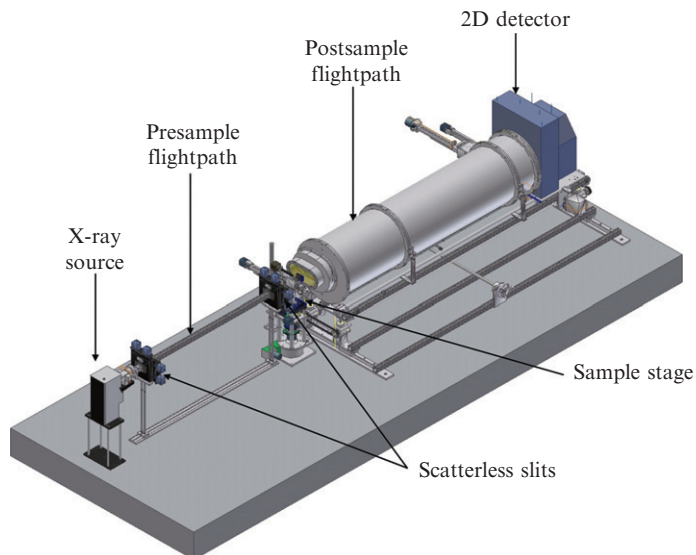
Figure 4.3 Layout of a microsource SAXS system. The spectrometer depicted is a Forvis custom-built instrument at UCLA CNSI. The microfocus sources, both sealed tube and rotating anode, give a brighter beam with lower total power than conventional rotating anode sources. The scatterless slits, made of a rectangular single-crystal substrate, for example, Si or Ge, bonded to a high-density metal base with a large taper angle ($>10°$), increase the usable flux by several folds (Li *et al.*, 2008).

respectively. The scattered intensity is collected using a MAR-Research (Hamburg) charge-coupled device detector (pixel size 79 µm). For in-house SAXS experiments, incident Cu Kα radiation ($\lambda = 1.54$ Å) from a Rigaku rotating-anode generator is monochromatized and focused using Osmic confocal multilayer optics and collimated to a final beam size of $\sim 0.8 \times 0.8$ mm^2. Scattered radiation is collected on a Bruker two-dimensional multiwire detector (pixel size 105 µm). All experiments are conducted at room temperature. No evidence of radiation damage to the samples is observed under the X-ray exposure levels used. For calibration, a capillary containing Millipore H_2O and an empty X-ray capillary are measured to assess the contribution of the solution and of the capillary itself. X-ray capillary containing dry silver behenate powder is measured to accurately and directly determine the sample to detector distance.

3.7. Translation of two-dimensional X-ray image to diffraction data

The detectors record the number of incident photons at each pixel position and generate two-dimensional diffraction images. The reciprocal lattice vector, q, is related to the pixel number by $q = (4\pi / \lambda)\sin \theta$, where 2θ is

the scattering angle and λ is the wavelength of the photon. The two-dimensional diffraction images are calibrated for beam center and detector angular tilt using a standard silver behenate sample. Silver behenate is strongly scattering with several well-defined diffraction peaks. The peak position of the first diffraction peak is used to calculate the sample to detector distance. The two-dimensional images are then radially integrated using Nika 1.2 (usaxs.xor.aps.anl.gov/staff/ilavsky/nika.html) data reduction package or FIT2D (www.esrf.eu/computing/scientific/FIT2D/). The diffracted intensity is plotted against q. The appearance of one or more sharp (Bragg) peaks in the low-angle region of the diffraction pattern helps identify the phase of the complex. The positions of the diffraction peaks are related to periodicity in the phase and the width of the peaks is related to the extent of this periodicity.

For detailed descriptions of X-ray diffraction data analysis procedures, we refer the reader to specialized references on the topic (Cullity, 1956; Guinier, 1994; Ladd and Palmer, 1994; Warren, 1990; Woolfson, 1997). A number of simple structures often occur in lipid mesophases. For example, the Lα lamellar phase consists of alternating layers of lipid bilayers and peptides, and its diffraction pattern has concentric equidistant rings centered at the origin. This quasi-one-dimensional periodic structure shows a series of peaks described by

$$q_n = \frac{2\pi}{d} n \tag{4.12}$$

where $n = 1, 2, 3$, etc. and d is the lamellar repeat distance of the one-dimensional lattice. The inverted hexagonal phase has cylindrical water channels, coated by inverse membrane monolayers, packed in a two-dimensional hexagonal lattice. The diffraction peaks are positioned at

$$q = \frac{4\pi}{\sqrt{3}a} \sqrt{h^2 + k^2 + hk} \tag{4.13}$$

where a is the distance between the centers of two neighboring water channels and h and k are the miller indices.

Cubic lipid phases have a more complex architecture. The lattice type can be identified by the characteristic ratios of the q positions of the Bragg peaks, given by

$$q = \frac{2\pi}{a} \sqrt{h^2 + k^2 + l^2} \tag{4.14}$$

where a is the cubic lattice constant and h, k, and l are the miller indices. The crystallographic space group to which the phase belongs is determined from

the systematic absences of peaks in the diffraction pattern. However, this is often not trivial, as only a few low-angle Bragg peaks are usually detected. This is due to the large thermal disorder inherent in liquid–crystalline phases, which strongly damps the intensities at larger diffraction angles. From unaligned samples, it is sometimes only possible to identify the cubic aspect from the systematic absences, leaving an ambiguity about the precise space group (Seddon and Templer, 1995; Winter and Jeworrek, 2009).

Figure 4.4 shows the X-ray diffraction data for the α-defensin Crp4 complexed with a 20:80 DOPS:DOPE membrane bilayer. The diffraction peaks have ratios √2:√3:√4:√6, which indicate the formation of a cubic Pn3m "double-diamond" lattice. The fitted slope of the plot between the measured peak positions and the corresponding Pn3m cubic indexation, $\sqrt{h^2 + k^2 + l^2}$, gives the lattice parameter of the cubic phase. The presence of the cubic phase indicates that Crp4 is able to induce negative Gaussian curvature in membranes, which is topologically required for pore formation.
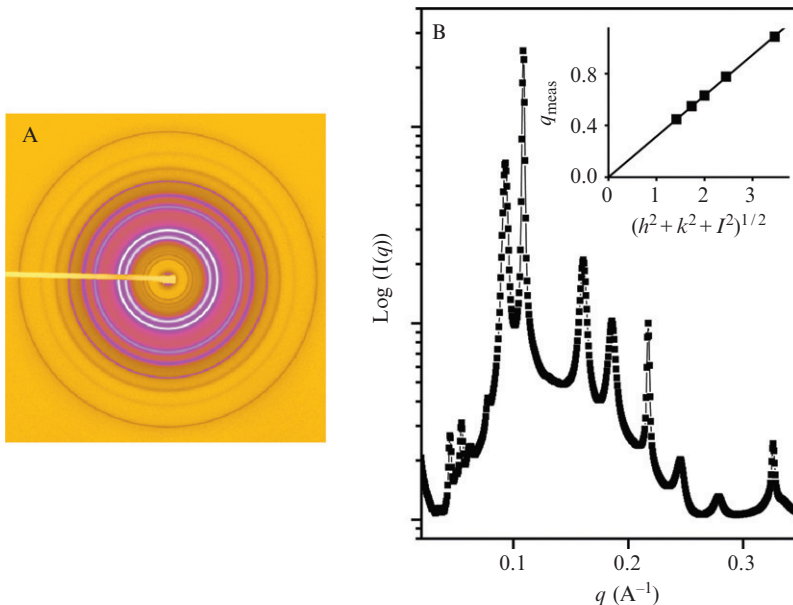
Figure 4.4   (A) Two-dimensional diffraction image for α-defensin Crp4 complexed with a 20:80 DOPS:DOPE membrane at a peptide–lipid molar ratio of 1/90. (B) Diffracted intensity $I(q)$ plotted against reciprocal lattice vector, q. The ratios of diffracted peak positions indicate formation of the Cubic *Pn3m* phase. The measured peak positions show good agreement with the corresponding *Pn3m* cubic indexation, $\sqrt{h^2 + k^2 + l^2}$ (inset).

4. SUMMARY

In this chapter, we show how SAXS methods, used to study soft condensed matter systems, can be adapted to investigate peptide–membrane interactions. Examining the structures of corresponding peptide–membrane complexes can help elucidate the mechanism of actions of AMPs and CPPs. Here, Crp4 is used as an illustrative example, but the method can be generalized to a broad range of membrane-active peptides.

ACKNOWLEDGMENTS

REFERENCES

Aley, S. B., Zimmerman, M., Hetsko, M., Selsted, M. E., and Gillin, F. D. (1994). Killing of *Giardia lamblia* by cryptdins and cationic neutrophil peptides. *Infect. Immun.* **62,** 5397–5403.

Als-Nielsen, J., and McMorrow, D. (2001). Elements of Modern X-ray Physics. John Wiley & Sons, Inc., New York.

Borenstein, L. A., Ganz, T., Sell, S., Lehrer, R. I., and Miller, J. N. (1991). Contribution of rabbit leukocyte defensins to the host response in experimental syphilis. *Infect. Immun.* **59,** 1368–1377.

Brogden, K. (2005). Antimicrobial peptides: Pore formers or metabolic inhibitors in bacteria? *Nat. Rev. Microbiol.* **3,** 238–250.

Chaikin, P., and Lubensky, T. (1995). Principles of Condensed Matter Physics. Cambridge University Press, Cambridge.

Cullity, B. (1956). Elements of X-Ray Diffraction. Addison-Wesley, Reading.

Cummings, J. E., Satchell, D. P., Shirafuji, Y., Ouellette, A. J., and Vanderlick, T. K. (2003). Electrostatically controlled interactions of mouse Paneth cell alpha-defensins with phospholipid membranes. *Aust. J. Chem.* **56,** 1031–1034.

Cummings, J. E., and Vanderlick, T. K. (2007). Kinetics of cryptdin-4 translocation coupled with peptide-induced vesicle leakage. *Biochemistry* **46,** 11882–11891.

Diamond, G., Zasloff, M., Eck, H., Brasseur, M., Maloy, W. L., and Bevins, C. L. (1991). Tracheal antimicrobial peptide, a cysteine–rich peptide from mammalian tracheal mucosa: Peptide isolation and cloning of a cDNA. *Proc. Natl. Acad. Sci. USA* **88,** 3952–3956.

El-Sayed, A., Futaki, S., and Harashima, H. (2009). Delivery of macromolecules using arginine-rich cell-penetrating peptides: Ways to overcome endosomal entrapment. *AAPS J.* **11,** 13–22.

Elliott, G., and O'Hare, P. (1997). Intracellular trafficking and protein delivery by a herpes virus structural protein. *Cell* **88,** 223–233.

Figueredo, S., Mastroianni, J. R., Tai, K. P., and Ouellette, A. J. (2010). Expression and purification of recombinant alpha-defensins and alpha-defensin precursors in *Escherichia coli*. *Methods Mol. Biol.* **618,** 47–60.

Frankel, A. D., and Pabo, C. O. (1988). Cellular uptake of the tat protein from human lmmunodeficiency virus. *Cell* **55,** 1189–1193.

Ganz, T. (2003). Defensins: Antimicrobial peptides of innate immunity. *Nat. Rev. Immunol.* **3,** 710–720.

Ganz, T., Selsted, M. E., Szklarek, D., Harwig, S. S., Daher, K., Bainton, D. F., and Lehrer, R. I. (1985). Defensins. Natural peptide antibiotics of human neutrophils. *J. Clin. Invest.* **76,** 1427–1435.

Green, M., and Loewenstein, P. M. (1988). Autonomous functional domains of chemically synthesized human immunodeficiency virus tat trans-activator protein. *Cell* **55,** 1179–1188.

Guinier, A. (1994). X-Ray Diffraction in Crystals, Imperfect Crystals, and Amorphous Bodies. Dover, New York.

Hancock, R. E. W., and Sahl, H.-G. (2006). Antimicrobial and host-defense peptides as new anti-infective therapeutic strategies. *Nat. Biotechnol.* **24,** 1551–1557.

Hickel, A., Danner-Pongratz, S., Amenitsch, H., Degovics, G., Rappolt, M., Lohner, K., and Pabst, G. (2008). Influence of antimicrobial peptides on the formation of nonlamellar lipid mesophases. *Biochim. Biophys. Acta* **1778,** 2325–2333.

Hristova, K., Selsted, M. E., and White, S. H. (1996). Interactions of monomeric rabbit neutrophil defensins with bilayers: Comparison with dimeric human defensin HNP-2. *Biochemistry* **35,** 11888–11894.

Huang, H. W. (2000). Action of antimicrobial peptides: Two-state model. *Biochemistry* **39,** 8347–8352.

Joliot, A., Pernelle, C., Deagostini-Bazin, H., and Prochiantz, A. (1991). Antennapedia homeobox peptide regulates neural morphogenesis. *Proc. Natl. Acad. Sci. USA* **88,** 1864–1868.

Keller, S., Gruner, S., and Gawrisch, K. (1996). Small concentrations of alamethicin induce a cubic phase in bulk phosphatidylethanolamine mixtures. *Biochim. Biophys. Acta* **1278,** 241–246.

Ladd, M., and Palmer, R. (1994). Structure Determination by X-Ray Crystallography. Plenum Press, New York.

Lehrer, R. I. (2004). Primate defensins. *Nat. Rev. Microbiol.* **2,** 727–738.

Lehrer, R. I. (2007). Multispecific myeloid defensins. *Curr. Opin. Hematol.* **14,** 16–21.

Lehrer, R. I., Barton, A., and Ganz, T. (1988). Concurrent assessment of inner and outer membrane permeabilization and bacteriolysis in *E. coli* by multiple-wavelength spectro-photometry. *J. Immunol. Methods* **108,** 153–158.

Lehrer, R. I., Selsted, M. E., Szklarek, D., and Fleischmann, J. (1983). Antibacterial activity of microbicidal cationic proteins 1 and 2, natural peptide antibiotics of rabbit lung macrophages. *Infect. Immun.* **42,** 10–14.

Li, Y., Beck, R., Huang, T., Choi, M. C., and Divinagracia, M. (2008). Scatterless hybrid metal-single-crystal slit for small-angle X-ray scattering and high-resolution X-ray dif-fraction. *J. Appl. Crystallogr.* **41,** 1134–1139.

Liang, H., Harries, D., and Wong, G. (2005). Polymorphism of DNA-anionic liposome complexes reveals hierarchy of ion-mediated interactions. *Proc. Natl. Acad. Sci. USA* **102,** 11173–11178.

Maemoto, A., Qu, X., Rosengren, K. J., Tanabe, H., Henschen-Edman, A., Craik, D. J., and Ouellette, A. J. (2004). Functional analysis of the {α}-defensin disulfide array in mouse cryptdin-4. *J. Biol. Chem.* **279,** 44188–44196.

Matsuzaki, K. (1999). Why and how are peptide-lipid interactions utilized for self-defense? Magainins and tachyplesins as archetypes. *Biochim. Biophys. Acta* **1462,** 1–10.

Matsuzaki, K., Sugishita, K.-I., Ishibe, N., Ueha, M., Nakata, S., Miyajima, K., and Epand, R. M. (1998). Relationship of membrane curvature to the formation of pores by magainin 2. *Biochemistry* **37,** 11856–11863.

Mishra, A., Gordon, V., Yang, L., Coridan, R., and Wong, G. (2008). HIV TAT forms pores in membranes by inducing saddle-splay curvature: Potential role of bidentate hydrogen bonding. *Angew. Chem. Intl. Ed.* **47,** 2986–2989.

Mitchell, D. J., Kim, D. T., Steinman, L., Fathman, C. G., and Rothbard, J. B. (2000). Polyarginine enters cells more efficiently than other polycationic homopolymers. *J. Pept. Res.* **56,** 318–325.

Ouellette, A. J. (2006). Paneth cell alpha-defensin synthesis and function. *Curr. Top. Microbiol. Immunol.* **306,** 1–25.

Ouellette, A. J., and Bevins, C. L. (2001). Paneth cell defensins and innate immunity of the small bowel. *Inflamm. Bowel Dis.* **7,** 43–50.

Prenner, E. J., Lewis, R. N. A. H., Neuman, K. C., Gruner, S. M., Kondejewski, L. H., Hodges, R. S., and McElhaney, R. N. (1997). Nonlamellar phases induced by the interaction of gramicidin S with lipid bilayers. A possible relationship to membrane-disrupting activity. *Biochemistry* **36,** 7906–7916.

Purdy Drew, K. R., Sanders, L. K., Culumber, Z. W., Zribi, O., and Wong, G. C. L. (2008). Cationic amphiphiles increase activity of aminoglycoside antibiotic tobramycin in the presence of airway polyelectrolytes. *J. Am. Chem. Soc.* **131,** 486–493.

Purdy, K. R., Bartles, J., and Wong, G. (2007). Structural polymorphism of the actin–espin system: A prototypical system of filaments and linkers in stereocilia. *Phys. Rev. Lett.* **98,** 058105.

Rädler, J., Koltover, I., Salditt, T., and Safinya, C. (1997). Structure of DNA-cationic liposome complexes: DNA intercalation in multilamellar membranes in distinct inter-helical packing regimes. *Science* **275,** 810–814.

Rajabi, M., de Leeuw, E., Pazgier, M., Li, J., Lubkowski, J., and Lu, W. (2008). The conserved salt bridge in human alpha-defensin 5 is required for its precursor processing and proteolytic stability. *J. Biol. Chem.* **283,** 21509–21518.

Rosengren, K. J., Daly, N. L., Fornander, L. M., Jonsson, L. M., Shirafuji, Y., Qu, X., Vogel, H. J., Ouellette, A. J., and Craik, D. J. (2006). Structural and functional characterization of the conserved salt bridge in mammalian paneth cell alpha-defensins: Solution structures of mouse Cryptdin-4 and (E15D)-Cryptdin-4. *J. Biol. Chem.* **281,** 28068–28078.

Rothbard, J. B., Jessop, T. C., and Wender, P. A. (2005). Adaptive translocation: The role of hydrogen bonding and membrane potential in the uptake of guanidinium-rich transporters into cells. *Adv. Drug Deliv. Rev.* **57,** 495–504.

Sanders, L., Guáqueta, C., Angelini, T., Lee, J., Slimmer, S., Luijten, E., and Wong, G. (2005). Structure and stability of self-assembled actin–lysozyme complexes in salty water. *Phys. Rev. Lett.* **95,** 108302.

Sanders, L., Xian, W., Guáqueta, C., Strohman, M., Vrasich, C., Luijten, E., and Wong, G. (2007). Control of electrostatic interactions between F-actin and genetically modified lysozyme in aqueous media. *Proc. Natl. Acad. Sci. USA* **104,** 15994–15999.

Satchell, D. P., Sheynis, T., Kolusheva, S., Cummings, J. E., Vanderlick, T. K., Jelinek, R., Selsted, M. E., and Ouellette, A. J. (2003a). Quantitative interactions between cryptdin-4 amino terminal variants and membranes. *Peptides* **24,** 1793–1803.

Satchell, D. P., Sheynis, T., Shirafuji, Y., Kolusheva, S., Ouellette, A. J., and Jelinek, R. (2003b). Interactions of mouse Paneth cell alpha-defensins and alpha-defensin precursors with membranes: Prosegment inhibition of peptide association with biomimetic membranes. *J. Biol. Chem.* **278,** 13838–13846.

Schmidt, N., Mishra, A., Lai, G., Davis, M., Sanders, L., Tran, D., Garcia, A., Tai, K., McCray, P., Ouellette, A., Selsted, M., and Wong, G. (2010a). Submitted.

Schmidt, N. W., Mishra, A., Lai, G. H., and Wong, G. C. L. (2010a). Arginine–rich cell-penetrating peptides. *FEBS Lett.* **584,** 1806–1813.

Schonwetter, B. S., Stolzenberg, E. D., and Zasloff, M. A. (1995). Epithelial antibiotics induced at sites of inflammation. *Science* **267,** 1645–1648.

Schutte, B. C., Mitros, J. P., Bartlettt, J. A., Walters, J. D., Jia, H. P., Welsh, M. J., Casavant, T. L., and McCray, P. B. (2002). Discovery of five conserved beta-defensin gene clusters using a computational search strategy. *Proc. Natl. Acad. Sci. USA* **99,** 2129–2133.

Seddon, J., and Templer, R. (1995). Polymorphism of lipid–water systems. *In* "Structure and Dynamics of Membranes: From Cell to Veiscles," (R. Lipowsky and E. Sackmann, eds.), Vol. 1. Elsevier, Amsterdam.

Selsted, M. E., Brown, D. M., Delange, R. J., and Lehrer, R. I. (1983). Primary structures of MCP-1 and MCP-2, natural peptide antibiotics of rabbit lung macrophages. *J. Biol. Chem.* **258,** 14485–14489.

Selsted, M. E., and Harwig, S. S. (1989). Determination of the disulfide array in the human defensin HNP-2. A covalently cyclized peptide. *J. Biol. Chem.* **264,** 4003–4007.

Selsted, M. E., and Ouellette, A. J. (2005). Mammalian defensins in the antimicrobial immune response. *Nat. Immunol.* **6,** 551–557.

Selsted, M. E., Tang, Y. Q., Morris, W. L., McGuire, P. A., Novotny, M. J., Smith, W., Henschen, A. H., and Cullor, J. S. (1993). Purification, primary structures, and anti-bacterial activities of beta-defensins, a new family of antimicrobial peptides from bovine neutrophils. *J. Biol. Chem.* **268,** 6641–6648.

Shai, Y. (1999). Mechanism of the binding, insertion and destabilization of phospholipid bilayer membranes by α-helical antimicrobial and cell non-selective membrane-lytic peptides. *Biochim. Biophys. Acta* **1462,** 55–70.

Shirafuji, Y., Tanabe, H., Satchell, D. P., Henschen-Edman, A., Wilson, C. L., and Ouellette, A. J. (2003). Structural determinants of procryptdin recognition and cleavage by matrix metalloproteinase-7. *J. Biol. Chem.* **278,** 7910–7919.

Som, A., Yang, L., Wong, G. C. L., and Tew, G. N. (2009). Divalent metal ion triggered activity of a synthetic antimicrobial in cardiolipin membranes. *J. Am. Chem. Soc.* **131,** 15102–15103.

Staudegger, E., Prenner, E. J., Kriechbaum, M., Degovics, G., Lewis, R. N. A. H., McElhaney, R. N., and Lohner, K. (2000). X-ray studies on the interaction of the antimicrobial peptide gramicidin S with microbial lipid extracts: Evidence for cubic phase formation. *Biochim. Biophys. Acta* **1468,** 213–230.

Warren, B. E. (1990). X-Ray Diffraction. Dover Publications, New York.

Wender, P. A., Galliher, W. C., Goun, E. A., Jones, L. R., and Pillow, T. H. (2008). The design of guanidinium-rich transporters and their internalization mechanisms. *Adv. Drug Deliv. Rev.* **60,** 452–472.

White, S. H., Wimley, W. C., and Selsted, M. E. (1995). Structure, function, and membrane integration of defensins. *Curr. Opin. Struct. Biol.* **5,** 521–527.

Winter, R., and Jeworrek, C. (2009). Effect of pressure on membranes. *Soft Matter* **5,** 3157.

Wong, G. (2006). Electrostatics of rigid polyelectrolytes. *Curr. Opin. Colloid Interface Sci.* **11,** 310–315.

Wong, G., Tang, J., Lin, A., Li, Y., Janmey, P., and Safinya, C. (2000). Hierarchical self-assembly of F-Actin and cationic lipid complexes: Stacked three-layer tubule networks. *Science* **288,** 2035–2039.

Woolfson, M. (1997). An Introduction to X-Ray Crystallography. Cambridge University Press, Cambridge.

Wu, Z., Li, X., de Leeuw, E., Ericksen, B., and Lu, W. (2005). Why is the Arg5–Glu13 salt bridge conserved in mammalian alpha-defensins? *J. Biol. Chem.* **280,** 43039–43047.

Yang, L., Gordon, V. D., Mishra, A., Som, A., Purdy, K. R., Davis, M. A., Tew, G. N., and Wong, G. C. L. (2007). Synthetic antimicrobial oligomers induce a composition–dependent topological transition in membranes. *J. Am. Chem. Soc.* **129,** 12141–12147.

Yang, L., Gordon, V. D., Trinkle, D. R., Schmidt, N. W., Davis, M. A., DeVries, C., Som, A., Cronan, J. E., Tew, G. N., and Wong, G. C. L. (2008). Mechanism of a prototypical synthetic membrane-active antimicrobial: Efficient hole-punching via interaction with negative intrinsic curvature lipids. *Proc. Natl. Acad. Sci. USA* **105,** 20595–20600.

Yang, L., Liang, H., Angelini, T. E., Butler, J., Coridan, R., Tang, J. X., and Wong, G. C. L. (2004). Self-assembled virus-membrane complexes. *Nat. Mater.* **3,** 615–619.

Zanetti, M. (2004). Cathelicidins, multifunctional peptides of the innate immunity. *J. Leukoc. Biol.* **75,** 39–48.

Zasloff, M. (2002). Antimicrobial peptides of multicellular organisms. *Nature* **415,** 389–395.

Zhu, S. (2008). Discovery of six families of fungal defensin-like peptides provides insights into origin and evolution of the CSalphabeta defensins. *Mol. Immunol.* **45,** 828–838.

Zweytick, D., Tumer, S., Blondelle, S. E., and Lohner, K. (2008). Membrane curvature stress and antibacterial activity of lactoferricin derivatives. *Biochem. Biophys. Res. Commun.* **369,** 395–400.